STScI | SPACE TELESCOPE SCIENCE INSTITUTE

Instrument Science Report COS 2021-03(v1)

Updated Flux Error Calculations for CalCOS

Christian I. Johnson[1], Rachel Plesha[1], Robert Jedrzejewski[1], Elaine Frazer[1], and Dzhuliya Dashtamirova[1]

[1] Space Telescope Science Institute, Baltimore, MD

26 April 2021

ABSTRACT

Recent reports indicated that the flux errors provided by CalCOS version 3.3.9 and earlier versions may be overestimated for low signal-to-noise ratio (S/N) COS FUV/NUV spectra. An investigation into this phenomenon confirmed that the error calculation method, which was based on the analytic approximations provided by Gehrels (1986), was not implemented as intended. Starting with CalCOS 3.3.10, flux errors are now calculated using a numerical approximation of the Gehrels (1986) analytic functions, and asymmetric errors are reported for `X1D`*,* `X1DSUM[N]`*, and* `X1DSUM` *files. The new method provides significantly reduced flux errors for low S/N spectra while leaving higher S/N data mostly unaffected. Four new columns are generated by CalCOS 3.3.10 for output 1D spectra, including a lower flux error and the three terms that are used to calculate the flux errors. For consistency with previous reductions, the* `ERROR` *column remains the upper flux error. The new columns increase transparency and permit CalCOS users to apply custom error calculations when desired.*

Operated by the Association of Universities for Research in Astronomy, Inc., for the National Aeronautics and Space Administration.

Contents

1. Introduction

CalCOS is a primarily Python-based software suite designed to perform common data reduction tasks (e.g., bad pixel masking; spectrum extraction; wavelength calibration; etc.) for ultraviolet (UV) spectra obtained with far-UV (FUV) and near-UV (NUV) channels of the Cosmic Origins Spectrograph (COS) on the Hubble Space Telescope (HST)[1]. Among the many products generated by CalCOS, the X1D, X1DSUM[N], and X1DSUM spectra are the most commonly used files for scientific research. The X1D files are the calibrated one dimensional spectra from individual exposures. Similarly, the X1DSUM[N] files are the combined spectra for all exposures taken at the same grating offset position (FP-POS; the "N" indicates the FP-POS value between 1 and 4), and the X1DSUM files are the final combined spectra for all exposures at a given grating and cenwave setting and within a given association. Recent investigations have reported that the CalCOS-reported flux errors are significantly larger than the empirical 1σ scatter observed in continuum regions for low signal-to-noise ratio (S/N) spectra, which suggests a problem may be present in the calculation of flux errors for individual exposures and/or the error propagation procedure. This instrument science report investigates the flux error calculation procedure for CalCOS 3.3.9 and describes revisions that have been made for CalCOS 3.3.10.

[1]The CalCOS source code is available at https://github.com/spacetelescope/calcos, and further details regarding data products are available in the COS Data Handbook at https://hst-docs.stsci.edu/cosdhb.

2. Background

2.1 Deriving CalCOS `X1D` Flux Errors Using Root-N Assumptions

Following the intended COS error calculation procedure outlined in Wilkinson et al. (2002), the net count rate for a given wavelength bin (N_i) is defined as:

$$N_i = \varepsilon_i(GC_i - BK_i), \tag{1}$$

where ε_i is the "inefficiency factor" [2], GC_i is the gross count rate per wavelength bin, and BK_i is the background count rate per wavelength bin. The net counts per wavelength bin can be determined through a similar relation that multiplies the rate terms on both sides of Equation 1 by the exposure time (t) to obtain:

$$N_i t = \varepsilon_i t(GC_i - BK_i) \rightarrow n_i = \varepsilon_i(gc_i - bk_i), \tag{2}$$

where the lower case n_i, gc_i, and bk_i variables represent the net, gross, and background counts, rather than the count rates. Since the net count rate is proportional to a source's flux, the CalCOS flux errors are formally calculated as an uncertainty in the net counts and then divided by the exposure time to get the net count rate errors.

Prior to CalCOS version 3.3.10, the `ERROR` arrays present in `X1D` files represented the symmetric flux errors calculated from the net count uncertainty derived from Equation 2. Assuming the terms in Equation 2 are not correlated and their associated errors are small, the net count variance for a given wavelength bin can be calculated as:

$$\sigma_{n_i}^2 = \left(\frac{\partial n_i}{\partial \varepsilon_i}\sigma_{\varepsilon_i}\right)^2 + \left(\frac{\partial n_i}{\partial gc_i}\sigma_{gc_i}\right)^2 + \left(\frac{\partial n_i}{\partial bk_i}\sigma_{bk_i}\right)^2, \tag{3}$$

where σ_{ε_i} is the error term associated with the flat-field response, σ_{gc_i} is the Poisson error on the `GCOUNTS` array, and σ_{bk_i} is the Poisson error on the `BACKGROUND` array multiplied by the exposure time (to convert the background count rate into background counts). The partial derivative terms in Equation 3 can be determined using Equation 2 as:

$$\frac{\partial n_i}{\partial \varepsilon_i} = gc_i - bk_i; \frac{\partial n_i}{\partial gc_i} = \varepsilon_i; \frac{\partial n_i}{\partial bk_i} = -\varepsilon_i, \tag{4}$$

[2]The inefficiency factor for a photon event is defined as the inverse of the flat-field response at a given pixel location multiplied by the live time value. The live time is a ratio of the number of events counted by the detector electronics compared to the number of events entering the system. See Wilkinson et al. (2002), the COS Instrument Handbook (https://hst-docs.stsci.edu/cosihb), and/or the COS Data Handbook (https://hst-docs.stsci.edu/cosdhb) for more details.

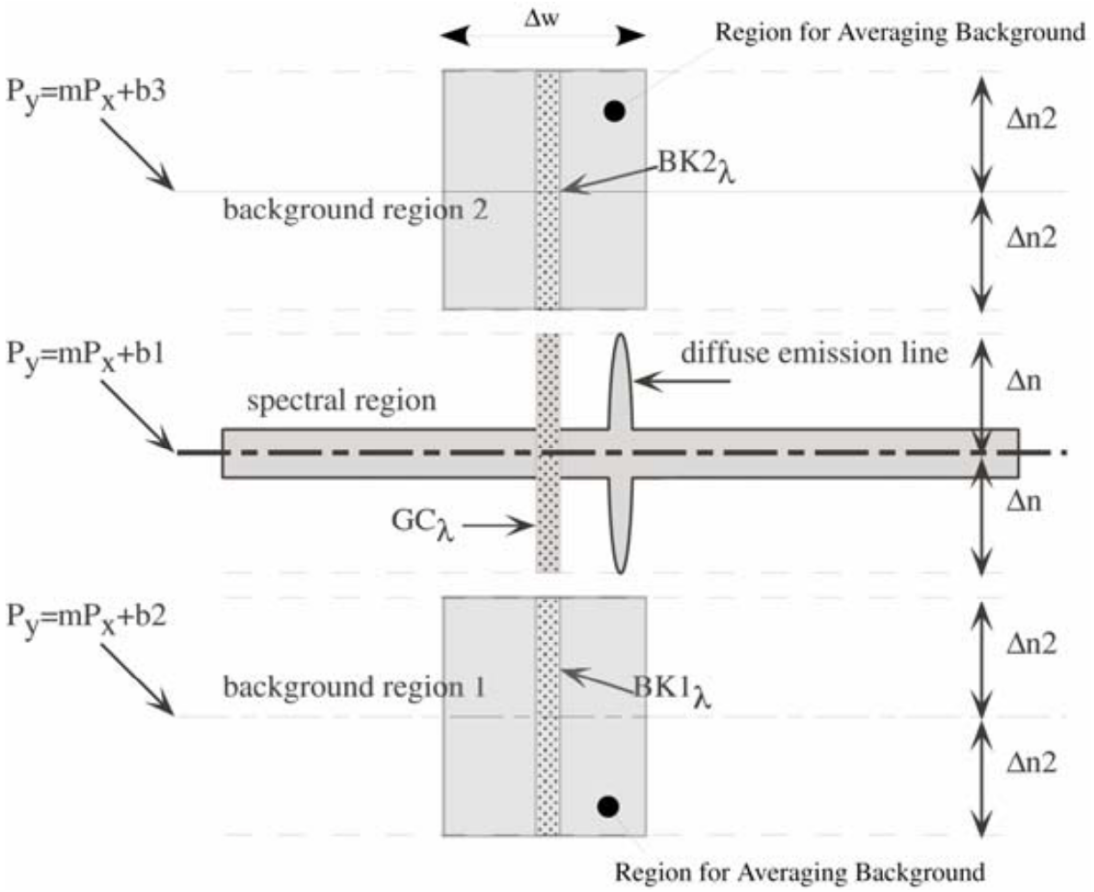

Figure 1. An illustration from Wilkinson et al. (2002) highlighting the various terms calculated during the spectrum extraction process.

which when inserted into Equation 3 gives:

$$\sigma_{n_i}^2 = [(gc_i - bk_i)\sigma_{\varepsilon_i}]^2 + (\varepsilon\sigma_{gc_i})^2 + (-\varepsilon\sigma_{bk_i})^2 \,. \tag{5}$$

Although equation 5 contains only three general terms, obtaining robust estimates for the σ_{ε_i}, σ_{gc_i}, and σ_{bk_i} variables may not be straight-forward. A full derivation of the first term in Equation 5 is beyond the scope of this document, but Wilkinson et al. (2002) show that the $(gc_i - bk_i)\sigma_{\varepsilon_i}$ term is well approximated by the relation:

$$[(gc_i - bk_i)\sigma_{\varepsilon_i}]^2 \approx \left(\frac{n_i}{E_j SNR_{\rm ff}}\right)^2 , \tag{6}$$

where n_i is the net count value per wavelength bin, E_j is the number of rows in the extraction height, and $SNR_{\rm ff}$ is the S/N of the flat-field image. For high count levels, Poisson distributions approach the Gaussian limit such that the gross and background

count error terms are well approximated by the familiar "root-N" method as:

$$\sigma_{gc_i} = \sqrt{gc_i}; \sigma_{bk_i} = \sqrt{\frac{\Delta n_1}{\Delta w \Delta n_2} bk_i}, \tag{7}$$

where Δn_1 is the spectrum extraction half height, Δw is the background extraction width, and Δn_2 is the background extraction half height (see Figure 1)[3]. Combining Equations 3-7 gives the net count variance of:

$$\sigma_{n_i}^2 = \left(\frac{n_i}{E_j SNR_{\text{ff}}}\right)^2 + (\varepsilon_i \sqrt{gc_i})^2 + \left(-\varepsilon_i \sqrt{\frac{\Delta n_1}{\Delta w \Delta n_2} bk_i}\right)^2, \tag{8}$$

which can be transformed into the net count rate error:

$$\sigma_{N_i} = \frac{1}{t}\sqrt{\left(\frac{N_i t}{E_j SNR_{\text{ff}}}\right)^2 + \left(\varepsilon_i \sqrt{GC_i t}\right)^2 + \left(-\varepsilon_i \sqrt{\frac{\Delta n_1}{\Delta w \Delta n_2} BK_i t}\right)^2}. \tag{9}$$

2.2 `X1D` Low Count Errors

Equation 9 represents the formal net count rate error for individual COS exposures (i.e., `X1D` files) under the usual root-N assumption. However, Equation 9 is only a reasonable estimator when the counts levels are high enough that the Poisson distributions approach the Gaussian limit. Figure 2 shows that Poisson distributions with low mean values are asymmetric and have tails that are skewed toward higher counts (since too few integers exist between 0 and the mean to form a symmetric distribution). Although no universally accepted solution exists for determining accurate upper/lower 1σ error bounds in the low count Poisson regime, a common approach in astronomical observations is to use the analytic approximations presented in Gehrels (1986). Specifically, a symmetric uncertainty based on the Gehrels (1986) 1σ upper confidence limit described by:

$$\sigma_{N;upper} = 1 + \sqrt{N + \frac{3}{4}}, \tag{10}$$

where N is the number of observed counts. However, Figure 3 shows that while Equation 10 is accurate for upper error bounds at all count levels, it provides a poor estimate of the lower errors when count levels are low. A more accurate approach is to use Equation 10 for the upper errors and separately apply the following relation from Gehrels (1986) for the lower errors:

$$\sigma_{N;lower} = N - \left[N\left(1 - \frac{1}{9N} - \frac{1}{3\sqrt{N}}\right)^3\right], \tag{11}$$

[3]These values can be found in the `XTRACTAB` reference file for lifetime positions 1-2 and the `TWOZXTAB` reference file for lifetime positions 3 and later.

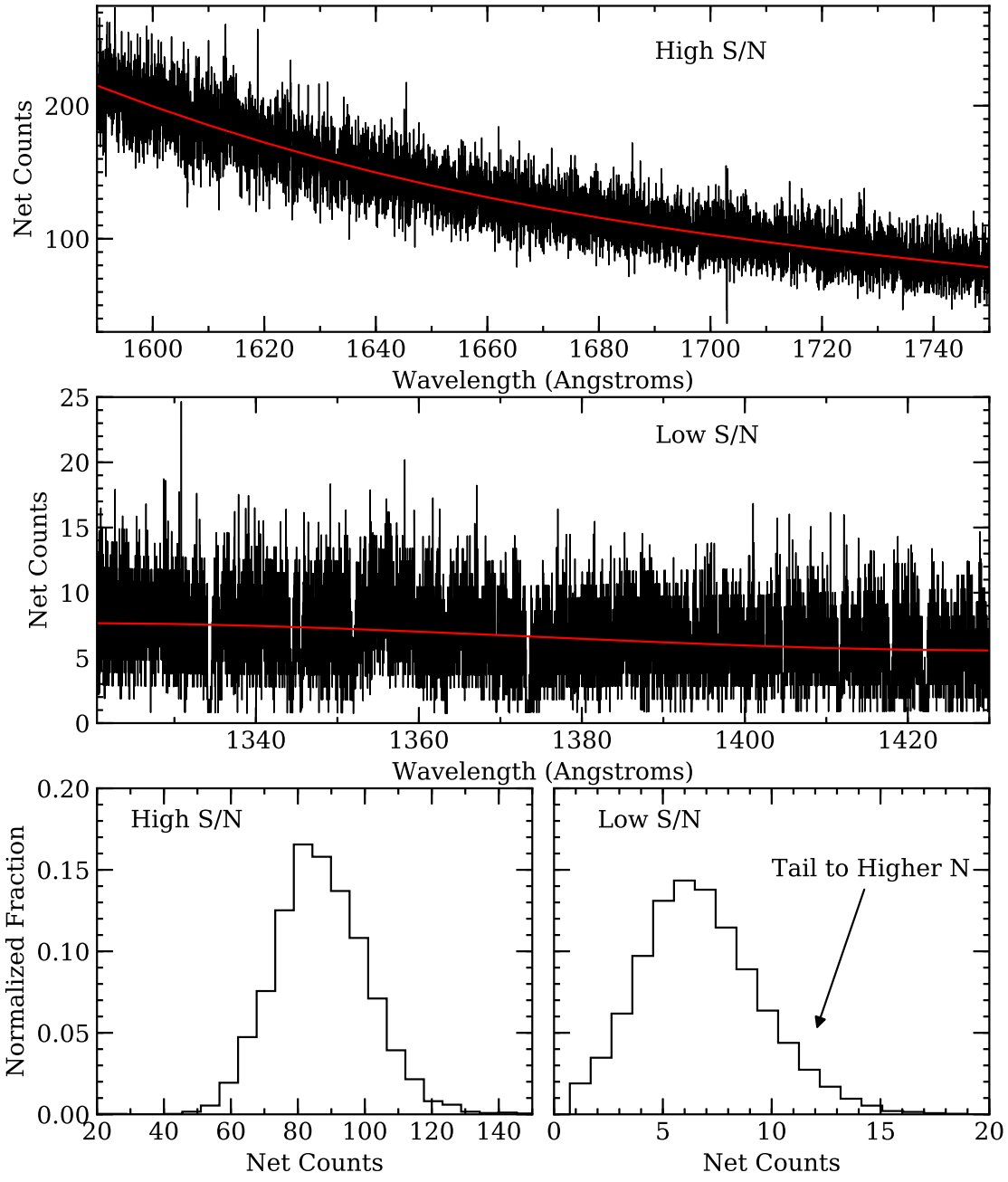

Figure 2. The top panel shows a high S/N, relatively featureless spectrum from Program ID 14910 that is contrasted against a similar low S/N spectrum from Program ID 13314 in the middle panel. For both panels the solid red line illustrates a low order polynomial fit through the data. The bottom left panel shows a histogram of the net count distribution from 1700-1760 Å for the high S/N case (top panel), and the bottom right panel shows a similar histogram from 1340-1420 Å for the low S/N case (middle panel). Note that the count distribution in the higher S/N case is more symmetric than the lower S/N case, which has a tail to higher count values.

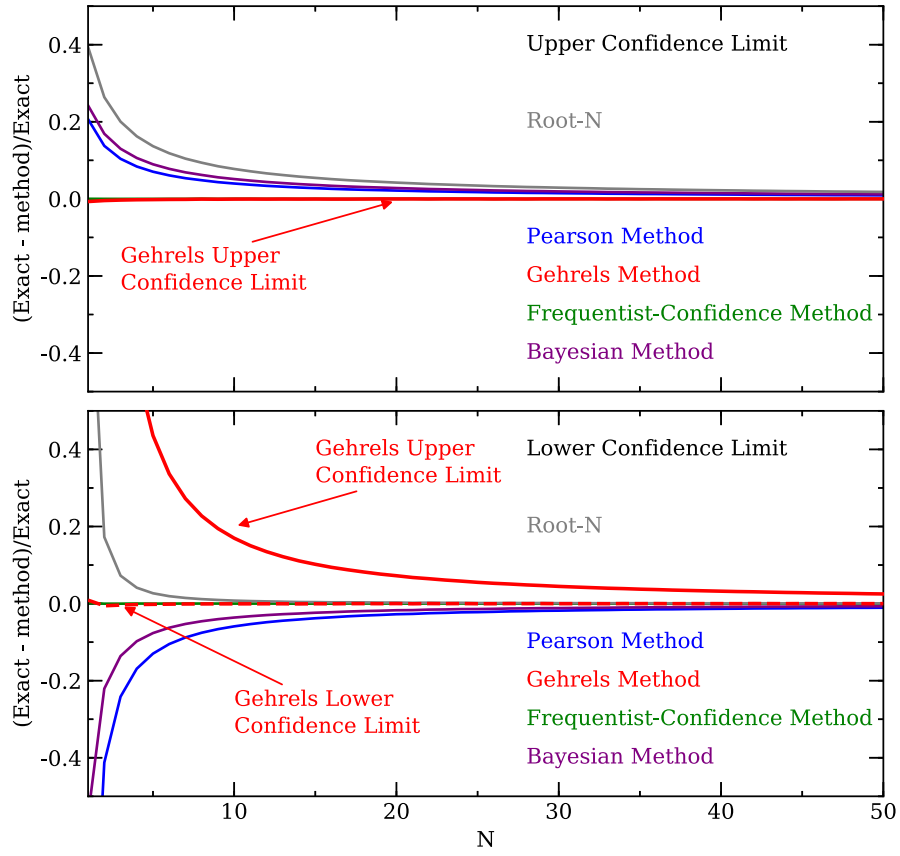

Figure 3. The top and bottom panels compare the fractional differences between various Poisson uncertainty estimate methods and the numerically solved one-sided 1σ upper/lower confidence limits presented in Tables 1 and 2 of Gehrels (1986), plotted as a function of integer counts (N). The gray lines are the usual root-N errors. However, the solid blue, red, green, and purple lines represent calculations using the `pearson`, `sherpagehrels`, `frequentist-confidence`, and `kraft-burrows-nousek` methods in the `astropy.stats.poisson_conf_interval` module, respectively. The bottom panel highlights differences in the lower error estimate when a symmetric uncertainty based on the Gehrels (1986) upper limit (solid red line) is used compared with the separate lower error calculation (dashed red line). Note that in both panels the "Frequentist-Confidence" calculation (solid green lines) follows the Gehrels (1986) upper/lower errors at all integer count levels. Additionally, all methods provide similar results for large count levels.

which is shown as the dashed red line in the bottom panel of Figure 3. Nevertheless, symmetry is often assumed for all count levels, as was the case for previous versions of CalCOS, with error bars determined solely from an implementation of Equation 10. The selection of Equation 10 over Equation 11 when adopting symmetric errors is often due to Equation 10 providing a more conservative (larger) error compared with Equation 11 alone.

Replacing the "root-N" σ_{gc_i} and σ_{bk_i} error terms[4] of Equation 7 with errors derived using Equation 10 changes Equation 9 to:

$$\sigma_{N_i} = \frac{1}{t}\left[\left(\frac{N_i t}{E_j SNR_{\rm ff}}\right)^2 + \left[\varepsilon_i\left(1+\sqrt{GC_i t+\frac{3}{4}}\right)\right]^2 + \left(-\varepsilon_i\left[1+\sqrt{\left(\frac{\Delta n_1}{\Delta w \Delta n_2}\right)BK_i t+\frac{3}{4}}\right]\right)^2\right]^{\frac{1}{2}}. \quad (12)$$

Equation 12 was the desired implementation for versions of CalCOS previous to 3.3.10; however, we demonstrate in Section 3.1 that this was not the actual equation used in CalCOS 3.3.9 and earlier versions.

3. New `X1D` Flux Error Calculations

3.1 Previous CalCOS Implementation

Data reduced with CalCOS versions previous to 3.3.10 intended to substitute Equation 10 in for the pure root-N implementation shown in Equation 7. However, the code instead combined Equations 9 and 10 to get:

$$\sigma_{N_i} = \frac{1}{t}\left(1+\sqrt{\left(\frac{N_i t}{E_j SNR_{\rm ff}}\right)^2 + \left[\varepsilon_i^2 t\left(GC_i + \left(\frac{\Delta n_1}{\Delta w \Delta n_2}\right)BK_i\right)\right] + \frac{3}{4}}\right). \quad (13)$$

Equation 13 is similar to Equation 12, but visual inspection of the two equations shows that the positions of the $+1$, $+\frac{3}{4}$, and ε_i factors are different. The primary issue with Equation 13 is that it applies Equation 10 to terms that have already been evaluated using root-N assumptions[5].

[4]Note that the first term related to the inefficiency factor retains the "root-N" assumption. See Wilkinson et al. (2002) for details.

[5]Note that the square root expression that arises from Equation 3 is not related to any Poisson distribution error estimates, and instead results from the first order Taylor series expansion of Equation 2.

In order to assess the differences between Equations 9 (root-N), 12 (intended use of Gehrels 1986 upper confidence limit), and 13 (previously adopted use of Gehrels 1986 upper confidence limit), it is instructive to simplify the net count rate error equations to only include the gross count rate term, which dominates for most COS observations. For example, Equation 13 reduces to:

$$\sigma_{N_i} \approx \frac{1}{t}\left(1 + \sqrt{\varepsilon_i^2 GC_i t + \frac{3}{4}}\right) \tag{14}$$

while Equations 9 (root-N) and 12 are simplified to:

$$\sigma_{N_i} \approx \frac{1}{t}\left(\varepsilon_i \sqrt{GC_i t}\right) \tag{15}$$

and

$$\sigma_{N_i} \approx \frac{1}{t}\left[\varepsilon_i \left(1 + \sqrt{GC_i t + \frac{3}{4}}\right)\right]. \tag{16}$$

Visual inspection of Equations 14 and 16 shows that the key difference is the location of the ε_i factor, which is placed inside the radical for Equation 14 and outside the Gehrels (1986) component for Equation 16. In most cases, ε_i is near unity so Equations 14 and 16 yield approximately the same result, and when ε_i is exactly one the two equations are identical. Similarly, the primary difference between Equations 15 and 16 are the extra $+1$ and $+\frac{3}{4}$ factors driven by adopting Equation 10.

The dashed blue lines in Figure 4 show the behavior of Equation 13 for low S/N (top panel) and high S/N (bottom panel) COS `X1D` spectra in regions that are mostly free of strong emission and absorption lines. While in both cases the upper confidence limits appear reasonable given the observational scatter between wavelength bins, the lower confidence limit distribution is only reasonable for the high S/N case. The reason for this is illustrated in the bottom panel of Figure 3, which shows that the Gehrels (1986) upper confidence limit analytic relation (Equation 10 here) diverges strongly from the separate Gehrels (1986) lower confidence limit equation when counts are below about 20. We therefore conclude that the flux errors in COS data are not symmetric for low S/N data, and aim to implement a modified error calculation procedure for CalCOS.

3.2 Selecting and Implementing an Appropriate Method for `X1D` Files

Numerous methods exist for calculating upper and lower confidence limits for Poisson distributions (e.g., Wilson & Hilferty 1931; Garwood 1936; Gehrels 1986; Kraft et al. 1991; Schwertman & Martinez 1994; Barker 2002; Maxwell 2011), and the appropriate choice can depend heavily on the problem one is solving. For simplicity and continuity, we aim to adopt only one method for determining 1σ upper and lower

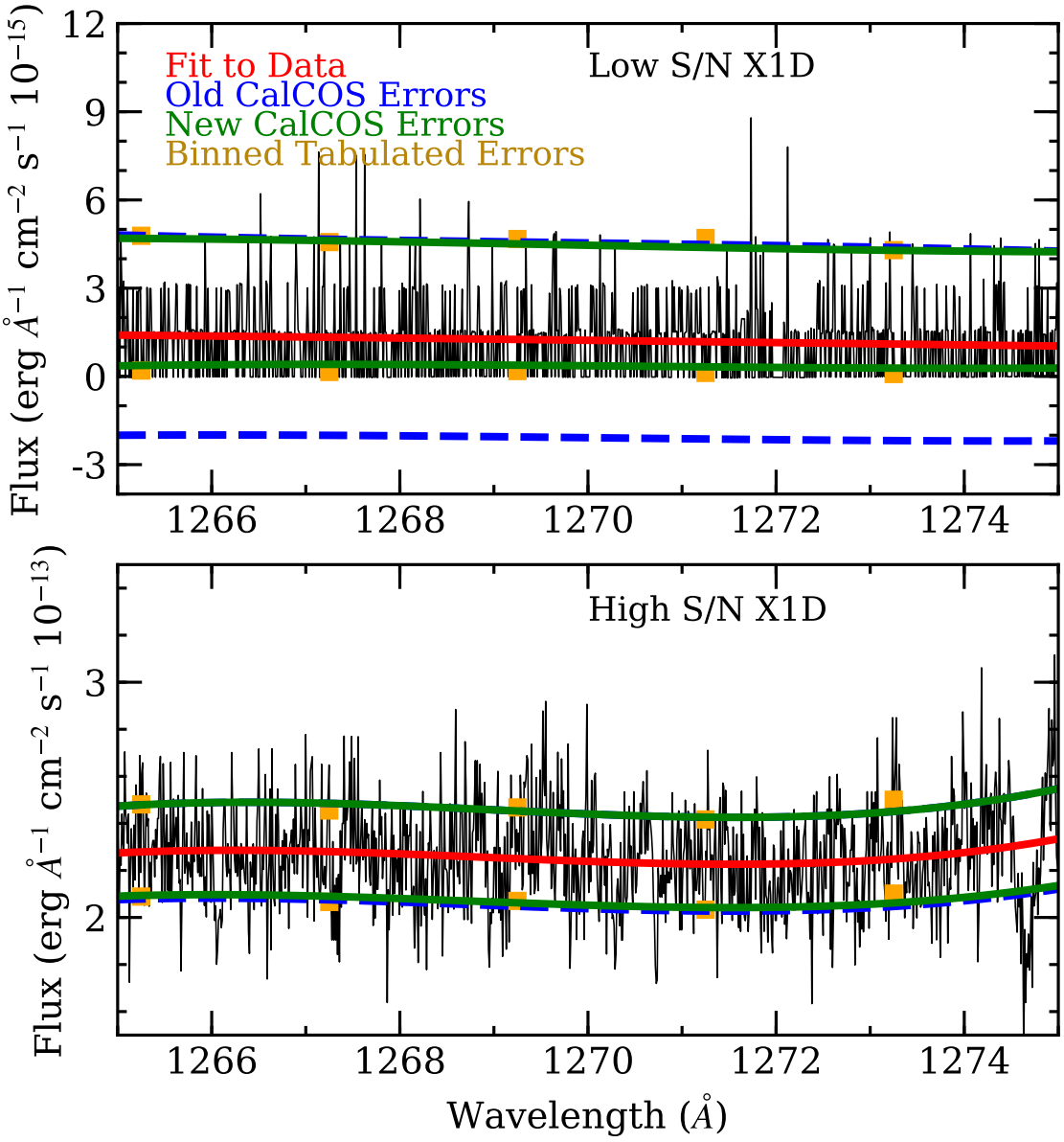

Figure 4. Upper and lower 1σ flux confidence limits are compared for sample low (top) and high (bottom) S/N COS spectra using the old (blue lines) and new (green lines) estimates. The dashed blue and solid green lines represent low order polynomial fits through the upper and lower flux error bounds. Note that the old and new pipeline estimates yield similar upper, but there is a substantial change in the lower limits, particularly at low S/N. For both panels, the solid red lines indicate low order polynomial fits to the data, and the orange squares represent the exact uncertainties in 1 Å bins using Tables 1 and 2 from Gehrels (1986).

flux errors with CalCOS, regardless of the count level. Furthermore, coding and scientific considerations suggest that CalCOS 3.3.10 should provide:

- accurate flux error calculations over a broad range of S/N regimes,
- reasonably fast computation since COS data are routinely reprocessed when new reference files or new versions of CalCOS are available,
- a simple coding interface that allows flexibility for improved error algorithms to be quickly substituted into the source code, and
- improved transparency regarding the individual terms contributing to the flux error calculations.

An investigation into various computation methods concluded that the `astropy.stats.poisson_conf_interval` package comprehensively addresses the desired code features outlined above, and also provides at least one method for obtaining accurate, asymmetric flux errors for a wide range of count levels. Figure 3 illustrates the computed upper/lower confidence limits from the available `poisson_conf_interval` methods and compares them against the tabulated "exact" values given in Gehrels (1986). From Figure 3 we can draw several conclusions:

- for count levels > 50, all methods give approximately the same upper/lower confidence limits as the Poisson distribution approaches the Gaussian limit,
- the standard root-N approximation begins to break down for $N < 30$ for upper confidence limits and $N < 5$ for lower confidence limits,
- using the Gehrels (1986) upper confidence limit and assuming symmetry leads to severely over-estimated lower confidence limits for $N < 20$,
- asymmetric Gehrels (1986) confidence limits provide accurate values for all count levels, and
- the asymmetric Gehrels (1986) and "Frequentist-Confidence" methods provide nearly identical confidence limits at all count levels.

The last bullet point above is particularly intriguing because unlike the `sherpagehrels` method, which only provides symmetric 1σ confidence limits based on Equation 10, the `frequentist-confidence` method explicitly provides asymmetric confidence limits that are equivalent to Equations 10 and 11. An

examination of the `frequentist-confidence` method's source code[6] in concert with Gehrels (1986) reveals why the two approaches yield similar values.

Equations 3-5 in Gehrels (1986) provide the basis for determining analytic approximations for Poisson confidence limits by noting the following relationship between Poisson sums and χ^2 distributions:

$$\sum_{x=0}^{n-1} \frac{\lambda^x e^{-\lambda}}{x!} = 1 - P(\chi^2 \mid \upsilon), \tag{17}$$

where P($\chi^2 \mid \upsilon$) is the χ^2 probability for υ degrees of freedom, $\chi^2 = 2\lambda$, and $\upsilon = 2n$. Furthermore, Gehrels (1986) notes that the upper and lower confidence limits can be derived from the χ^2 probability distribution function as:

$$P(2\lambda_u \mid 2n + 2) = CL \tag{18}$$

and

$$P(2\lambda_l \mid 2n) = 1 - CL, \tag{19}$$

respectively, with CL representing the confidence level (e.g., see also Equations 1-2 of Gehrels 1986) and λ_u/λ_l the upper/lower confidence limits. While Equations 10 and 11 provide analytic approximations for λ_u and λ_l in the special case of CL = 0.8413 (1σ), Gehrels (1986) also notes that the confidence limits can be calculated using percentage point tables of the χ^2 distribution. The `frequentist-confidence` method performs this calculation with:

```
alpha = scipy.stats.norm.sf(sigma)
conf_interval =
np.array([0.5 * scipy.stats.chi2(2 * n).ppf(alpha),
          0.5 * scipy.stats.chi2(2 * n + 2).isf(alpha)]).
```

Specifically, the lower confidence limit is numerically calculated from the χ^2 percentage point function while the upper confidence limit is determined from the χ^2 inverse survival function. A comparison between the source code above and Equations 18-19 highlights that the two approaches are equivalent. Note that the `alpha` parameter is approximately 0.1587 when $\sigma = 1$. The behavior of the code above is shown via the green lines in Figure 3.

Defining $f_{u,l}(N)$ as the upper/lower errors provided by the `frequentist-confidence` code, the net count rate uncertainty for an `X1D` file

[6]The source code is available at: https://docs.astropy.org/en/stable/_modules/astropy/stats/funcs.html.

can be determined by modifying Equation 12 to read:

$$\sigma_{u,l;N_i} = \frac{1}{t}\sqrt{\left(\frac{N_i t}{E_j SNR_{\rm ff}}\right)^2 + \left[\varepsilon_i f_{u,l}(GC_i t)\right]^2 + \left[-\varepsilon_i f_{u,l}\left(\frac{\Delta n_1}{\Delta w \Delta n_2} BK_i t\right)\right]^2}, \quad (20)$$

where $\sigma_{u,l;N_i}$ are the upper and lower net count rate error values per wavelength bin. Note that the `frequentist-confidence` code returns the upper (λ_u) and lower (λ_l) confidence limits, which are converted into upper/lower errors using:

$$\sigma_u = \lambda_u - N \quad (21)$$

and

$$\sigma_l = N - \lambda_l, \quad (22)$$

respectively, where N is the relevant count value. For COS `X1D` files produced with CalCOS 3.3.10, the upper and lower flux errors generated by Equation 20 are reported in the `ERROR` and `ERROR_LOWER` columns, respectively. Note that we retain the `ERROR` column name, rather than changing it to `ERROR_UPPER`, for consistency with previous CalCOS releases.

In order to increase transparency and aid users in implementing customized error calculation procedures, `X1D` files now include three additional columns:

$$VARIANCE\_FLAT_i \equiv \left(\frac{N_i t}{E_j SNR_{\rm ff}}\right)^2, \quad (23)$$

$$VARIANCE\_COUNTS_i \equiv \varepsilon_i^2 GC_i t, \quad (24)$$

and

$$VARIANCE\_BKG_i \equiv \varepsilon_i^2 \left(\frac{\Delta n_1}{\Delta w \Delta n_2} BK_i t\right), \quad (25)$$

where the exposure time (t), net count rate (N_i), gross count rate (GC_i), and background count rate (BK_i) values are available via the `EXPTIME`, `NET`, `GROSS`, and `BACKGROUND` data columns, respectively. Simple arithmetic can be used to determine the numerical values of the ε_i, $E_j SNR_{\rm ff}$, and $\frac{\Delta n_1}{\Delta w \Delta n_2}$ terms in each wavelength bin [7]. This information can then be combined to replace the $f_{u,l}$ function in Equation 20 with one of the user's choice. For example, if one desired symmetric root-N errors then $f_{u,l}$

[7]Note that the $SNR_{\rm ff}$ information is also available in the `FLATFILE` reference file as a header keyword.

would be the square root operator and visual inspection of Equations 20, 23, 24, and 25 shows that:

$$\sigma_{u,l;N_i} = \frac{1}{t}(VARIANCE\_FLAT_i + VARIANCE\_COUNTS_i + VARIANCE\_BKG_i)^{\frac{1}{2}}, \tag{26}$$

is identical to Equation 9.

4. New `X1DSUM[N]` and `X1DSUM` Flux Error Calculations

4.1 Previous CalCOS Implementation

For single exposures (e.g., `X1D` files), the calculated flux per wavelength bin is directly proportional to the observed net count rate. However, `X1DSUM[N]` and `X1DSUM` files often combine two or more spectra derived from exposures with different integration times. In the simplest case where multiple consecutive spectra are taken with the same spectrograph settings and combined, the merged flux values could be determined via a weighted average as:

$$F_\lambda = \frac{\sum_{i=1}^{N} F_{\lambda,i} t_i}{\sum_{i=1}^{N} t_i}, \tag{27}$$

where N is the number of exposures being combined, F_λ is the final flux per wavelength bin, $F_{\lambda,i}$ is the flux per wavelength bin per exposure (i), and t_i is the exposure time for each contributing image. Similarly, the propagated flux error associated with Equation 27 would be:

$$\sigma_{F_\lambda} = \frac{1}{\sum_{i=1}^{N} t_i} \sqrt{\sum_{i=1}^{N} (t_i \sigma_{\lambda,i})^2}, \tag{28}$$

where $\sigma_{\lambda,i}$ is the flux uncertainty for each wavelength bin in each image.

In practice, the relationship between wavelength and pixel space is not constant between images (e.g., combining different FP-POS) so the individual exposures must be resampled onto a common wavelength grid. As a result, Equations 27 and 28 are actually implemented as:

$$F_\lambda = \frac{\sum_{i=1}^{N} [(F_{\lambda,i} \cdot p_{\lambda,i} \cdot w_{\lambda,i}) + (F_{\lambda+1,i} \cdot q_{\lambda+1,i} \cdot w_{\lambda+1,i})]}{\sum_{i=1}^{N} [(p_{\lambda,i} \cdot w_{\lambda,i}) + (q_{\lambda+1,i} \cdot w_{\lambda+1,i})]} \tag{29}$$

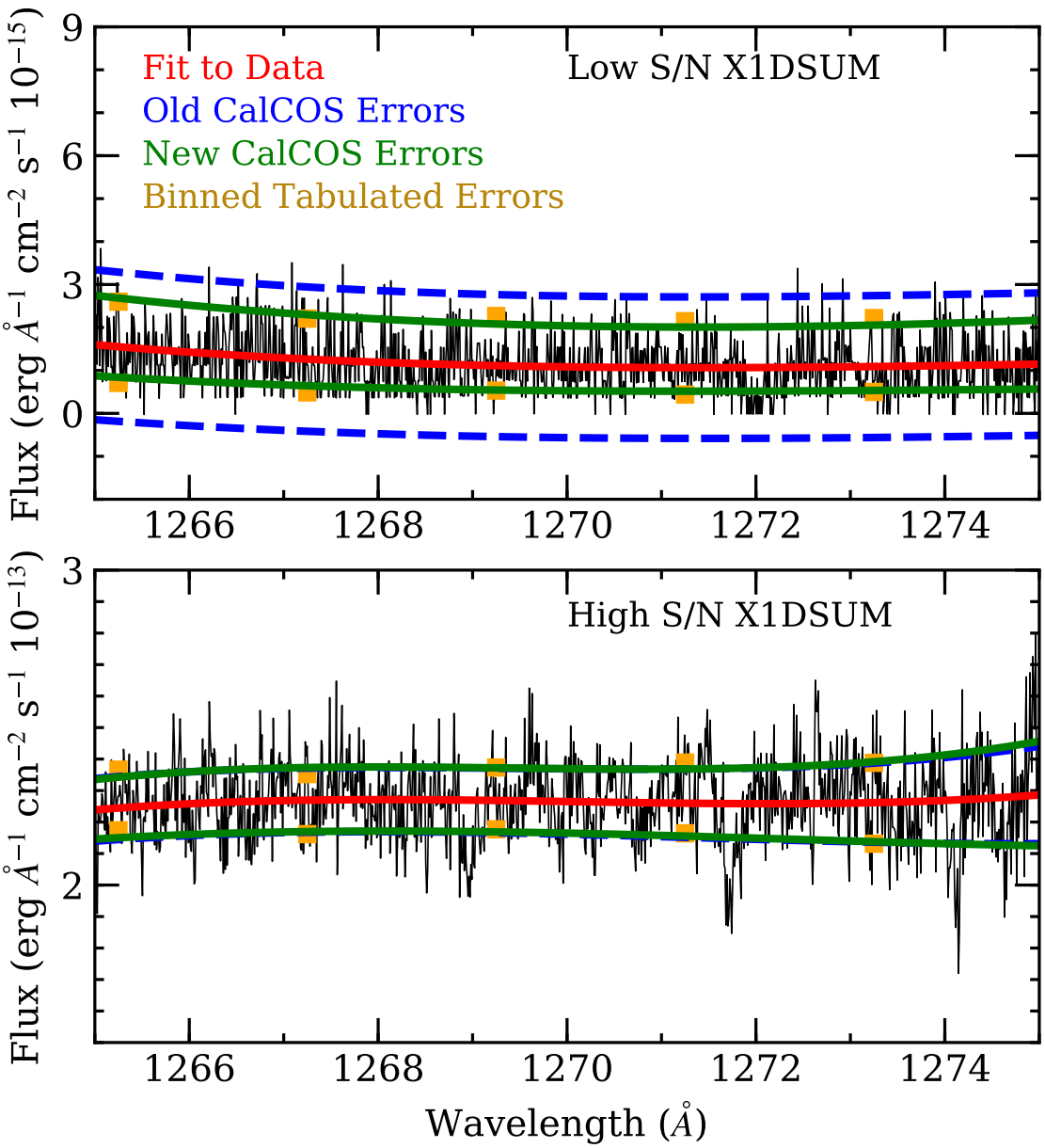

Figure 5. A similar plot to Figure 4 except the behavior of `X1DSUM` files are shown instead of comparing `X1D` files. Note the significant decrease in the magnitude of the errors for CalCOS 3.3.10 (solid green lines), especially at low S/N, compared with CalCOS 3.3.9 (dashed blue lines).

and

$$\sigma_{F_\lambda} = \frac{1}{\sum_{i=1}^{N} \left[(p_{\lambda,i} w_{\lambda,i}) + (q_{\lambda+1,i} w_{\lambda+1,i})\right]} \sqrt{\sum_{i=1}^{N} \left[(\sigma_{\lambda,i} p_{\lambda,i} w_{\lambda,i}) + (\sigma_{\lambda+1,i} q_{\lambda+1,i} w_{\lambda+1,i})\right]^2} \tag{30}$$

where the $p_{\lambda,i}$ and $q_{\lambda+1,i}$ coefficients sum to unity and represent the wavelength overlap from each observed wavelength bin and its adjacent neighbor, respectively, into the final spectrum. The $p_{\lambda,i}$ and $q_{\lambda+1,i}$ terms serve as linear interpolation flux weights since the input spectrum wavelength bins will rarely overlap directly with the resampled output wavelength bins. The $w_{\lambda,i}$ and $w_{\lambda+1,i}$ coefficients represent additional weights that account for data quality flags (`DQ_WGT`), exposure times (t_i), and flat-field ($FF_{\lambda,i}$) contributions as:

$$w_{\lambda,i} = DQ\_WGT_{\lambda,i} \cdot t_i \cdot FF_{\lambda,i} \tag{31}$$

and

$$w_{\lambda+1,i} = DQ\_WGT_{\lambda+1,i} \cdot t_i \cdot FF_{\lambda+1,i}, \tag{32}$$

respectively.

Figure 5 shows that although Equation 30 provides reasonable error estimates for high S/N X1DSUM data, the errors are too large compared to the intrinsic observational scatter in low S/N data.

4.2 New CalCOS Implementation

For versions of CalCOS previous to 3.3.10, the $\sigma_{\lambda,i}$ and $\sigma_{\lambda+1,i}$ values from Equation 30 would have been derived using Equation 13. However, several problems exist for this approach:

- we showed in Section 3 that Equation 13 is generally not correct.
- Figures 2 and 3 highlight that Poisson distributions become strongly asymmetric when count levels are low.
- Equation 30 does not include covariance terms that naturally arise due to the wavelength interpolation of `X1D` spectra being combined (e.g., Carnall 2017).

The first two bullet points are addressed by replacing Equation 13 with the naturally asymmetric Equation 20. However, this introduces a new problem because asymmetric errors cannot be combined in the same way as symmetric errors (i.e., Equation 28 is no longer valid). Although a common practice, upper and lower asymmetric errors cannot generally be added together separately in quadrature to obtain combined final

upper/lower error values (e.g., Barlow 2004). Therefore, a new error estimation procedure is required for X1DSUM[N] and X1DSUM files.

Calculating exact combined flux errors is not possible with the current CalCOS code, but we provide here a description of the adopted approximation scheme that exhibits the desired behavior. For CalCOS 3.3.10, the VARIANCE_FLAT, VARIANCE_COUNTS, and VARIANCE_BKG terms from Equations 23-25 are treated as "equivalent counts" contributed by the flat-field, source, and background in each image. Using this approximation, we can utilize a similar wavelength interpolation algorithm as described in Section 4.1 and apply it to the equivalent count terms as:

$$v_{flat,\lambda} = \sum_{i=1}^{N}([(VARIANCE\_FLAT_{\lambda,i} \cdot p_{\lambda,i} \cdot DQ\_WGT_{\lambda,i}) + (VARIANCE\_FLAT_{\lambda+1,i} \cdot q_{\lambda+1,i} \cdot DQ\_WGT_{\lambda+1,i})] \frac{1}{\sqrt{(p_{\lambda,i} \cdot DQ\_WGT_{\lambda,i})^2 + (q_{\lambda+1,i} \cdot DQ\_WGT_{\lambda+1,i})^2}}), \quad (33)$$

$$v_{counts,\lambda} = \sum_{i=1}^{N}([(VARIANCE\_COUNTS_{\lambda,i} \cdot p_{\lambda,i} \cdot DQ\_WGT_{\lambda,i}) + (VARIANCE\_COUNTS_{\lambda+1,i} \cdot q_{\lambda+1,i} \cdot DQ\_WGT_{\lambda+1,i})] \frac{1}{\sqrt{(p_{\lambda,i} \cdot DQ\_WGT_{\lambda,i})^2 + (q_{\lambda+1,i} \cdot DQ\_WGT_{\lambda+1,i})^2}}), \quad (34)$$

and

$$v_{bkg,\lambda} = \sum_{i=1}^{N}([(VARIANCE\_BKG_{\lambda,i} \cdot p_{\lambda,i} \cdot DQ\_WGT_{\lambda,i}) + (VARIANCE\_BKG_{\lambda+1,i} \cdot q_{\lambda+1,i} \cdot DQ\_WGT_{\lambda+1,i})] \frac{1}{\sqrt{(p_{\lambda,i} \cdot DQ\_WGT_{\lambda,i})^2 + (q_{\lambda+1,i} \cdot DQ\_WGT_{\lambda+1,i})^2}}), \quad (35)$$

where $v_{flat,\lambda}$, $v_{count,\lambda}$, and $v_{bkg,\lambda}$ are the interpolated equivalent count values in each wavelength bin originating from the flat-field, source, and background. The weights are the same as those described in Section 4.1. The normalization factors in Equations 33-35 are designed to roughly account for the covariance between adjacent wavelength bins during interpolation. The normalization factors vary smoothly between 1 (when only a single X1D bin contributes to an interpolated bin) and $\sqrt{2}$ (when two adjacent pixels contribute equally). A more formal treatment of covariance may be implemented in future CalCOS releases, but in practice one pixel usually dominates in

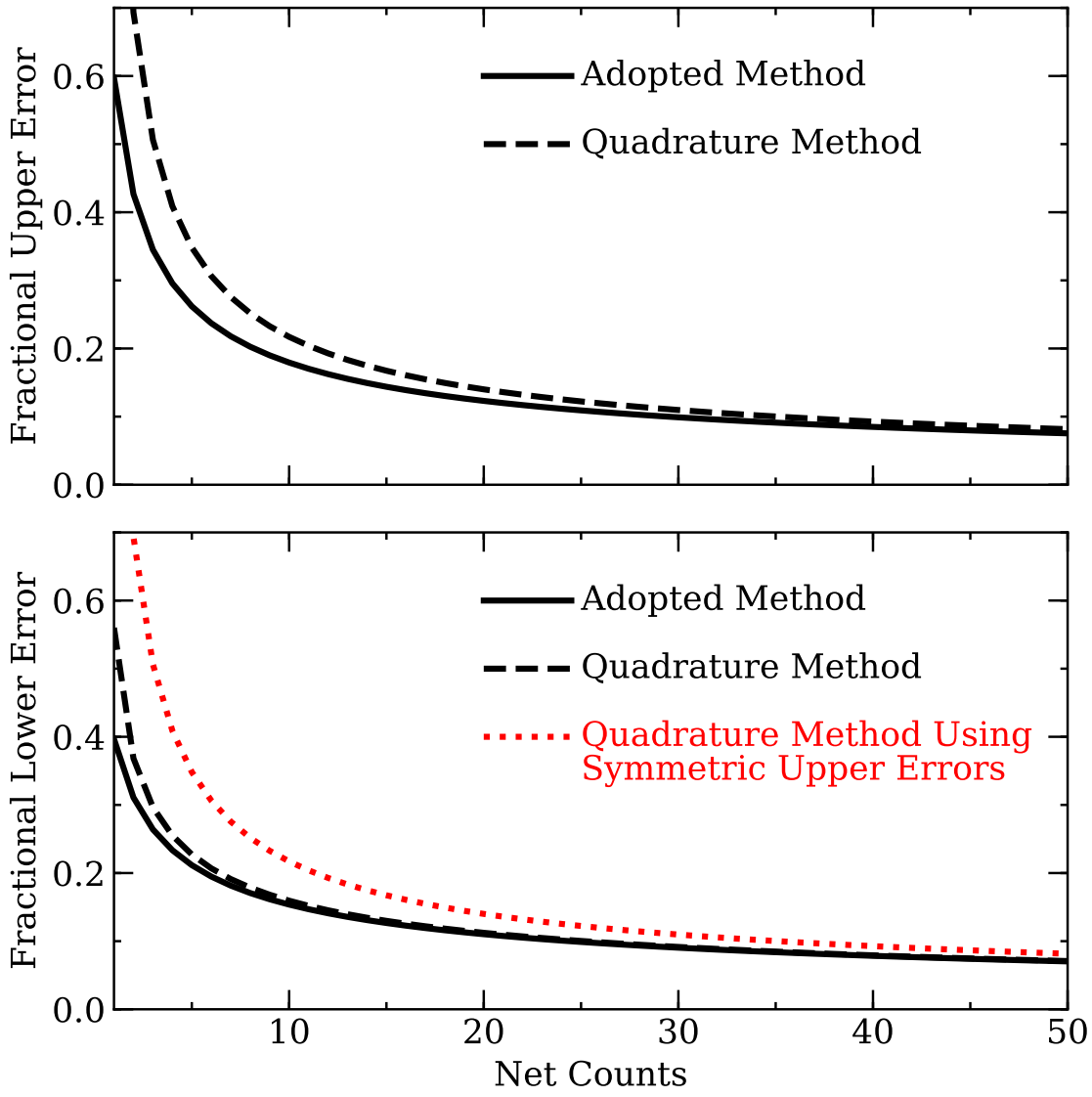

Figure 6. Sample calculations are shown comparing the new adopted method for determining `X1DSUM[N]` and `X1DSUM` net count errors (solid black lines) to the previous method of adding individual exposure errors in quadrature. The top and bottom panels illustrate the behavior of the upper and lower fractional errors, respectively. The dotted red line in the bottom panel shows the behavior of the old quadrature method that assumed symmetric errors based on the upper Gehrels (1986) limit. Note that all of the methods converge to approximately the same value for count values exceeding ~ 30.

the interpolation procedure. Note that Equations 33, 34, 35 represent the values given in the VARIANCE_FLAT, VARIANCE_COUNT, and VARIANCE_BKG columns of X1DSUM[N] and X1DSUM files, respectively.

Summing the contributions from Equations 33-35 gives an estimate of the total number of interpolated equivalent counts from all sources as:

$$v_{sum,\lambda} = v_{flat,\lambda} + v_{counts,\lambda} + v_{bkg,\lambda}. \tag{36}$$

The upper and lower effective count uncertainties are then calculated as:

$$\sigma_{v_{sum},\lambda;u,l} = f_{u,l}(v_{sum,\lambda}), \tag{37}$$

where $f_{u,l}$ is the `frequentist-confidence` method described in Section 3.2. The equivalent count error is then converted into an upper/lower flux error and reported in the ERROR and ERROR_LOWER columns of X1DSUM[N] and X1DSUM files.

Figure 6 shows that the adopted method provides the desired behavior such that Equation 37 produces significantly smaller upper/lower errors than Equation 30 (implementation from previous CalCOS versions) at low S/N and approaches Equation 30 at high S/N. The figure also shows that the adopted procedure generates smaller lower flux errors, especially at very low S/N, compared to an implementation of Equation 30 that (incorrectly) adds asymmetric errors independently in quadrature. Furthermore, Figure 5 shows that the new implementation better encapsulates the observational scatter of continuum regions in low S/N observations but does not significantly alter high S/N errors from previous CalCOS reductions.

We remind users that the errors produced by the methods outlined above for combined spectra are only approximations. Projects requiring a detailed understanding of all errors may need to substitute in custom error calculation routines (e.g., using the information provided in the new data columns) or run Monte Carlo simulations.

After adopting the code changes described above for X1DSUM[N] and X1DSUM files, we discovered that the flux errors were unusually small for background dominated spectra. The problem was traced to the conversion from count rate errors to flux errors, but appears to only significantly affect low S/N, background dominated NUV spectra (i.e., FUV data and all X1D flux errors are not affected by this issue). We are currently testing a patch that will be included in a future CalCOS version.

5. Summary

We present a detailed investigation into the previously adopted philosophy of calculating CalCOS flux errors for COS FUV/NUV X1D, X1DSUM[N], and X1DSUM

files. Following reports that the flux errors reported by CalCOS 3.3.9 and earlier versions may be too large for low S/N data, we discovered that the desired algorithm was not implemented as intended. Furthermore, assumptions such as symmetric errors begin to break down in the low count regime, and improved error estimates may be obtained by allowing asymmetric distributions. For CalCOS 3.3.10, we found that the `Frequentist-Confidence` method, which is part of the `astropy.stats.poisson_conf_interval` package, provides a simple coding interface while returning flux errors that are equivalent to those derived from the Gehrels (1986) analytic functions. Comparisons between the new and old CalCOS versions showed a significant reduction in the flux error values for low S/N data while leaving higher S/N data unaffected.

Starting with CalCOS 3.3.10, `X1D`, `X1DSUM[N]`, and `X1DSUM` files contain four new columns that increase transparency regarding flux error calculations, and also permit users to substitute customized routines. The first new column is labeled `ERROR_LOWER`, and provides the lower flux error estimate for each wavelength bin. For consistency with previous CalCOS reductions, the `ERROR` column remains the upper flux error. The three additional new columns are called `VARIANCE_FLAT`, `VARIANCE_COUNTS`, and `VARIANCE_BKG`, and provide information about the individual error terms. Since asymmetric errors cannot be propagated easily and the adopted wavelength interpolation scheme can introduce non-negligible flux covariance, the flux errors provided by `X1DSUM[N]` and `X1DSUM` files are now estimated using the total number of contributing equivalent counts for each pixel.

Acknowledgements

We are grateful to the COS team for many helpful comments and discussions.

Change History for COS ISR 2021-03

Version 1: 26 April 2021- Original Document

References

Barker, L., 2002, The American Statistician, 56, 86
Barlow, R., 2004, arXiv:physics/0406120
Carnall, C., 2017, arXiv:1705.05165
Garwood, F., 1936, Biometrika, 28, 437
Gehrels, N., 1986, ApJ, 303, 336
Kraft, R. P., Burrows, D. N., & Nousek, J. A., 1991, AJ, 374, 344
Maxwell, E. A., 2011, arXiv:1102.0822
Schwertman, N. C. & Martinez, R. A. 1994, Communication in Statistics — Theory

and Methods, 23, 1507
Wilkinson, E., Ebbets, D., Morse, J. A., et al., COS-01-0003, 2002
Wilson, E. B. & Hilferty, M. M., 1931, Proceedings of the National Academy of Sciences, 17, 684